Supporting Information

Shaw et al. 10.1073/pnas.1105941108

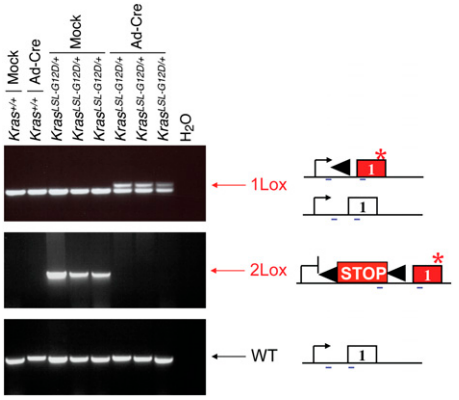

Fig. S1. Complete recombination of the *K-ras*$^{LSL\text{-}G12D}$ allele in MEFs after Adenoviral-Cre (Ad-Cre) infection. PCR genotyping of control (*K-ras*$^{+/+}$) and *K-ras*$^{LSL\text{-}G12D/+}$ MEFs before and after Ad-Cre–mediated recombination. One control and three representative *K-ras*$^{LSL\text{-}G12D/+}$ MEF lines are shown. (*Right*) Wild-type *K-ras* allele and the genomic confirmation of the *K-ras*$^{LSL\text{-}G12D/+}$ allele before (2Lox) and after (1Lox) recombination. Specific PCRs confirm complete loss of the 2Lox band and gain of the 1Lox band after infection of *K-ras*$^{LSL\text{-}G12D/+}$ MEF lines with Ad-Cre.

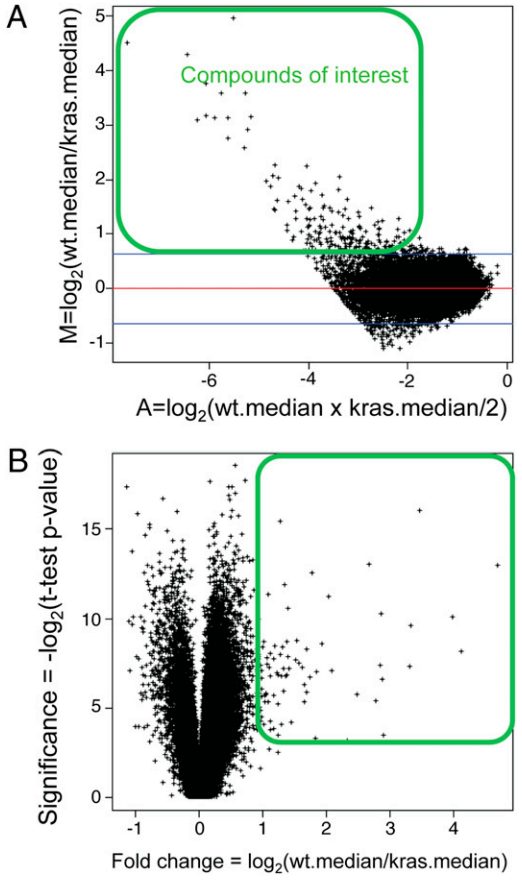

Fig. S2. Alternative graphical representation of primary screening results. (*A*) MvA plot showing an overview of the distribution of data. In simplified terms, the *y* axis represents fold change in viability between wild-type and K-ras mutant cells due to a specific compound. The greater the selectivity for mutant cells, the larger the M score. The *x* axis represents the product of the wild-type and mutant viability scores. Of note, compounds with selectivity for wild-type cells are not shown in this plot. (*B*) Plot of significance based on *P* values vs. fold change. Differential effects on cell viability were considered statistically significant if the *P* value based on *t* test was <0.05.

Compound	Structure	IC50 (μM) Wild-type	IC50 (μM) $Kras^{G12D}$
TP	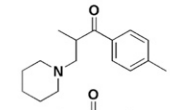	>40	20
LP	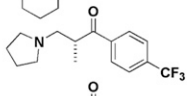	16	4
EP	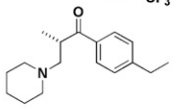	64	48
2-127	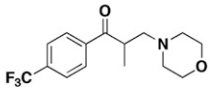	20	15
2-131	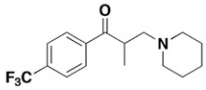	40	20
2-132	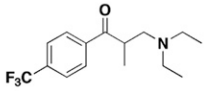	30	30
2-133	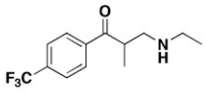	>40	40
2-123	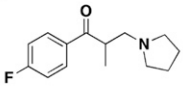	>40	40
2-146	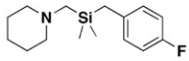	>40	>40
2-147	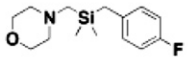	>40	>40
2-148	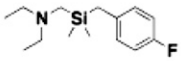	>40	>40
E10	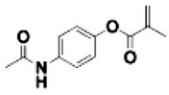	20	5

Fig. S3. Structure-function relationships. Shown are tolperisone (TP) and 10 TP-like derivatives. Lanperisone (LP) and eperisone (EP) are commercially available. The other TP-like derivatives were synthesized. IC_{50} values were estimated using the CTG viability assay after 48 h of drug treatment. Results shown are representative of three independent experiments.

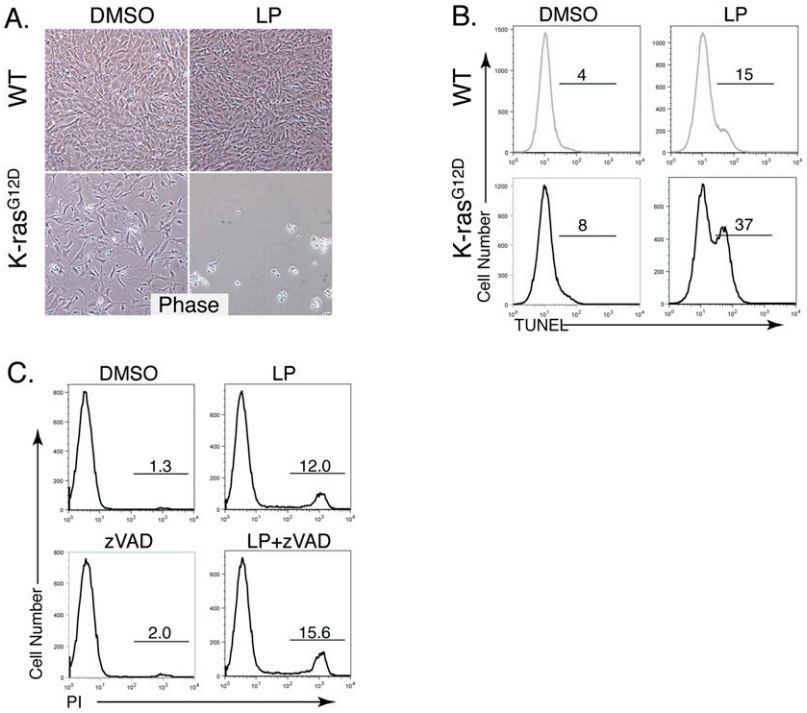

Fig. S4. LP induces enhanced caspase-independent death of *K-ras*^{G12D}-expressing cells. (*A*) LP (20 mM, 6 h) induced phenotypes associated with death selectively in *Mox-Cre;K-ras*^{G12D} MEFs. (*B*) LP (10 mM, 24 h) induces increased cell death of *Mox-Cre;K-ras*^{G12D}-expressing MEFs as assessed by flow cytometric analysis for TUNEL. (*C*) Caspase inhibition with zVAD (25 min pretreatment) does not block LP (20 mM, 6 h)-induced death of *Mox-Cre;K-ras*^{G12D}-expressing cells (assessed by flow cytometric analysis for PI).

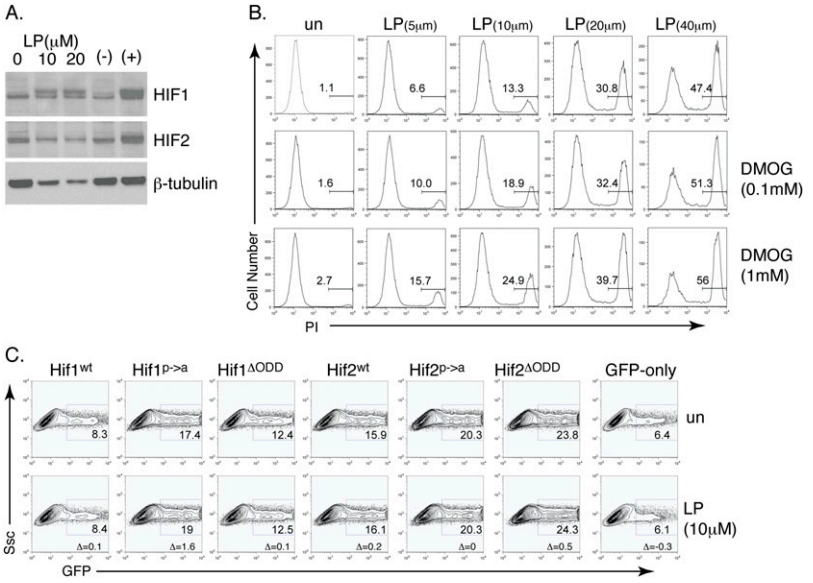

Fig. S5. Pharmacological and molecular modulation of HIF activity does not negatively impact LP-induced death. (*A*) LP treatment induces HIF-1 protein. Negative control [untreated (–)] and positive control [hypoxia (+)] lanes are shown. β-tubulin shows loading. (*B*) LP-induced death (6 h) of *Mox-Cre;K-ras*^{G12D}-expressing fibroblasts is not blocked by the prolyl-4-hydroxylase inhibitor DMOG. Percentage of dead (PI+) cells across a LP titration is shown. (*C*) Expression of active or dominant-negative HIF-1 and HIF-2 does not affect LP-induced death (6 h). *Mox-Cre;K-ras*^{G12D}-expressing fibroblasts were cotransfected with a GFP expression plasmid and the indicated HIF expression plasmids. Cells were then treated with LP or left untreated (un). If active or dominant negative HIF expression enhanced or reduced LP-induced death, the percentage of GFP+ cells in the LP-treated samples would be expected to be reduced or increased respectively. No such effects of exogenous HIF expression were observed.

A

Rank	Compound	Mean	Enrichment N	Score	p-value
1	parthenolide	0.841	4	0.986	<0.00001
3	ciclopirox	0.791	4	0.975	<0.00001
4	Lomustine	0.728	4	0.969	<0.00001
5	phenoxybenzamine	0.784	4	0.966	<0.00001
6	15-delta prostaglandin J2	0.772	15	0.848	<0.00001
7	geldanamycin	0.582	15	0.676	<0.00001
8	thioridazine	0.47	20	0.629	<0.00001
9	tanespimycin	0.524	62	0.583	<0.00001
10	trichostatin A	0.452	182	0.581	<0.00001
11	vorinostat	0.525	12	0.672	0.00002
12	MG-262	0.733	3	0.977	0.00004
13	F0447-0125	0.663	4	0.931	0.00004
14	5155877	0.699	4	0.92	0.00004
15	alvespimycin	0.429	12	0.656	0.00004
16	fluphenazine	0.392	18	0.519	0.00004
18	prochlorperazine	0.334	16	0.544	0.0001
19	niclosamide	0.564	5	0.828	0.00032
20	monorden	0.353	22	0.425	0.00036
21	STOCK1N-35215	0.684	3	0.934	0.00046
22	pyrvinium	0.435	6	0.753	0.00058
23	resveratrol	0.373	9	0.633	0.00058
24	clioquinol	0.49	5	0.81	0.0006
27	genistein	0.325	17	0.455	0.00112
28	5707885	0.531	4	0.834	0.00115
30	rottlerin	0.581	3	0.906	0.00174
31	thiostrepton	0.685	4	0.82	0.00183
32	oxyphenbutazone	0.617	4	0.819	0.00193
34	trifluoperazine	0.398	16	0.444	0.00207
35	methylbenzethonium Cl	0.413	6	0.694	0.00213
36	mefloquine	0.571	5	0.754	0.00216
37	ciclosporin	0.488	6	0.686	0.00242
38	Prestwick-642	0.462	4	0.809	0.00247
39	calmidazolium	0.708	2	0.959	0.00284

B

Rank	Compound	Dose	Cell Line	Score
4	parthenolide	16 μM	MCF7	0.945
6	parthenolide	16 μM	MCF7	0.916
62	parthenolide	16 μM	PC3	0.763
88	parthenolide	16 μM	HL60	0.74

C

Rank	Compound	Dose	Cell Line	Score
2	15-delta prostaglandin J2	10 μM	MCF7	0.97
3	15-delta prostaglandin J2	10 μM	MCF7	0.954
5	15-delta prostaglandin J2	10 μM	MCF7	0.925
7	15-delta prostaglandin J2	10 μM	MCF7	0.908
11	15-delta prostaglandin J2	10 μM	MCF7	0.877
12	15-delta prostaglandin J2	10 μM	HL60	0.861
14	15-delta prostaglandin J2	10 μM	MCF7	0.858
30	15-delta prostaglandin J2	10 μM	MCF7	0.822
37	15-delta prostaglandin J2	10 μM	HL60	0.804
80	15-delta prostaglandin J2	10 μM	PC3	0.749
102	15-delta prostaglandin J2	10 μM	HL60	0.729
380	15-delta prostaglandin J2	10 μM	PC3	0.587
486	15-delta prostaglandin J2	10 μM	PC3	0.557
536	15-delta prostaglandin J2	10 μM	MCF7	0.539
1035	15-delta prostaglandin J2	10 μM	SKMEL5	0.442

D

Rank	Compound	Dose	Cell Line	Score
15	geldanamycin	1 μM	MCF7	0.854
18	geldanamycin	1 μM	MCF7	.849
51	geldanamycin	1 μM	MCF7	.777
75	geldanamycin	1 μM	MCF7	.754
118	geldanamycin	1 μM	MCF7	.715
133	geldanamycin	1 μM	MCF7	.702
154	geldanamycin	1 μM	MCF7	.686
192	geldanamycin	1 μM	MCF7	.671
197	geldanamycin	1 μM	MCF7	.669
218	geldanamycin	1 μM	MCF7	.663
558	geldanamycin	1 μM	HL60	.532
768	geldanamycin	1 μM	PC3	.489
1492	geldanamycin	1 μM	HL60	.371
2068	geldanamycin	1 μM	PC3	0
2167	geldanamycin	1 μM	HL60	0

E

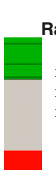

Rank	Compound	Dose	Cell Line	Score
297	erastin	20 μM	PC3	0.627
1239	erastin	20 μM	PC3	0.41
1847	erastin	20 μM	MCF7	0.303
1943	erastin	20 μM	MCF7	0.263

Fig. S6. CMAP analysis of LP treatment gene expression signatures. (*A*) Compounds showing high positive connectivity with LP treatment of K-ras mutant MEFs. Of note, LP treatment of wild-type MEFs showed qualitatively similar results. Mean refers to mean connectivity score of multiple instances of the same compound in the CMAP data set; *n*, number of instances of the identical compound in CMAP data set; the enrichment score reflects extent to which instances of a given compound are overrepresented among compound instances with the highest CMAP connectivity scores; *P* value reflects probability of obtaining the enrichment observed by chance (obtained by 100,000 random permutations of compound instances). (*B–E*) CMAP data for individual instances of parthenolide (*B*), 15-δ-prostaglandin J2 (*C*), geldanamycin (*D*), and erastin (*E*). In each figure, the red-green vertical bar depicts the list of all compound instances in the CMAP database, ranked according to their connectivity with the expression signature of LP-treated K-ras MEFs. Compound instances with the most positive connectivities are at the top of the list (green); compound instances with the most negative connectivities are at the bottom of the list (red). Within the red-green bar, each horizontal line depicts the rank of the compound instances described in the table (*Right*). The dose, cell line, and connectivity score are listed for each compound instance.

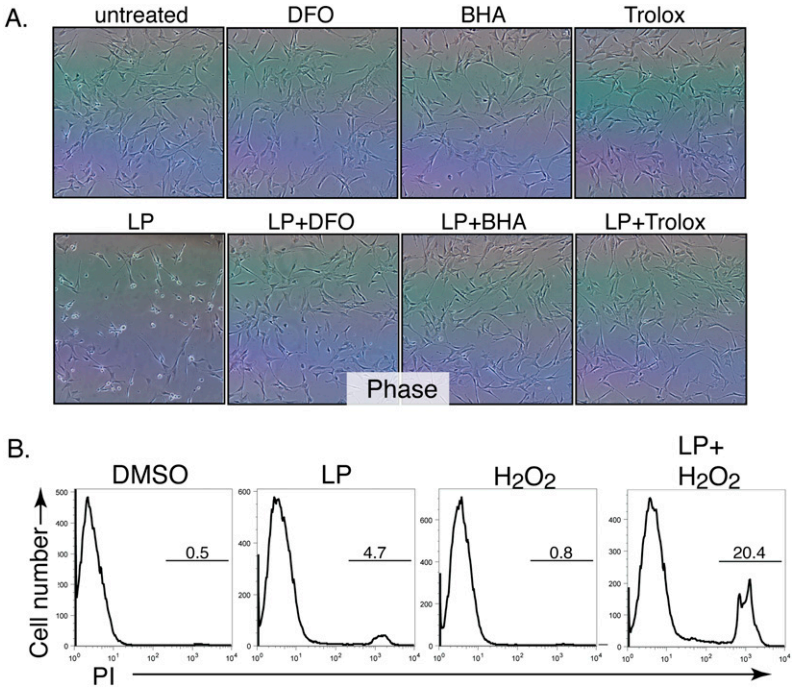

Fig. S7. Synergy of lanperisone with the oxidant hydrogen peroxide. (*A*) Suppression of LP-mediated cell death by pretreatment with antioxidants, as shown by phase contrast microscopy. *K-ras*^{G12D} MEFs were pretreated with DMSO, DFO, BHA, or Trolox and then exposed to 20 μM LP. (*B*) LP (20 mM) and H_2O_2 (100 mM) synergize to induce cell death of *Mox-Cre;K-ras*^{G12D} MEFs as assessed by flow cytometric analysis for PI. A 6-h time point is shown. Similar results were obtained comparing control *p53*$^{-/-}$ to *K-ras*^{G12D}*;p53*$^{-/-}$ MEFs.

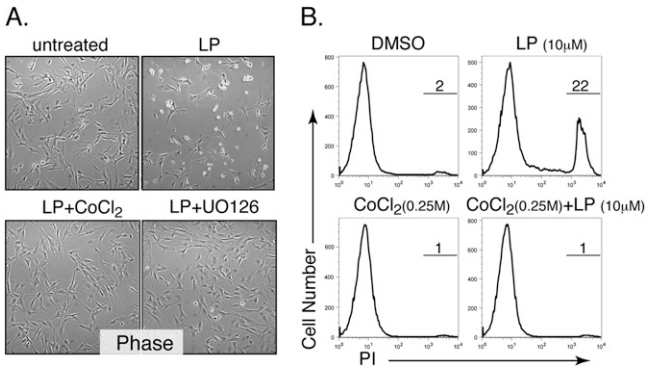

Fig. S8. Lanperisone-induced death is Mek- and iron-dependent. (*A*) Morphological changes induced by LP treatment in *Mox-Cre;K-ras*^{G12D}-expressing MEFs are blocked by treatment with CoCl2 or UO126. (*B*) LP-induced cell death of *Mox-Cre;K-ras*^{G12D}-expressing cells is blocked by CoCl2 (assessed by flow cytometric analysis for PI).

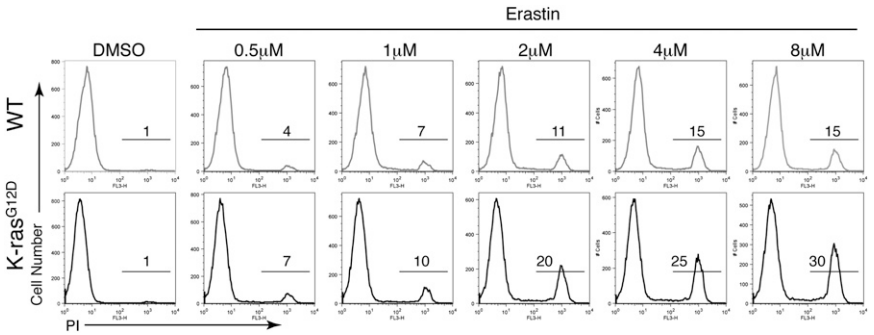

Fig. S9. Preferential killing of oncogenic K-ras–expressing MEFs by erastin. Erastin induces increased cell death of *Mox-Cre;K-ras*^{G12D}-expressing MEFs as assessed by flow cytometric analysis for PI. Concentration of erastin is shown. Data are representative of two MEF lines of each genotype at a 6-h time point.

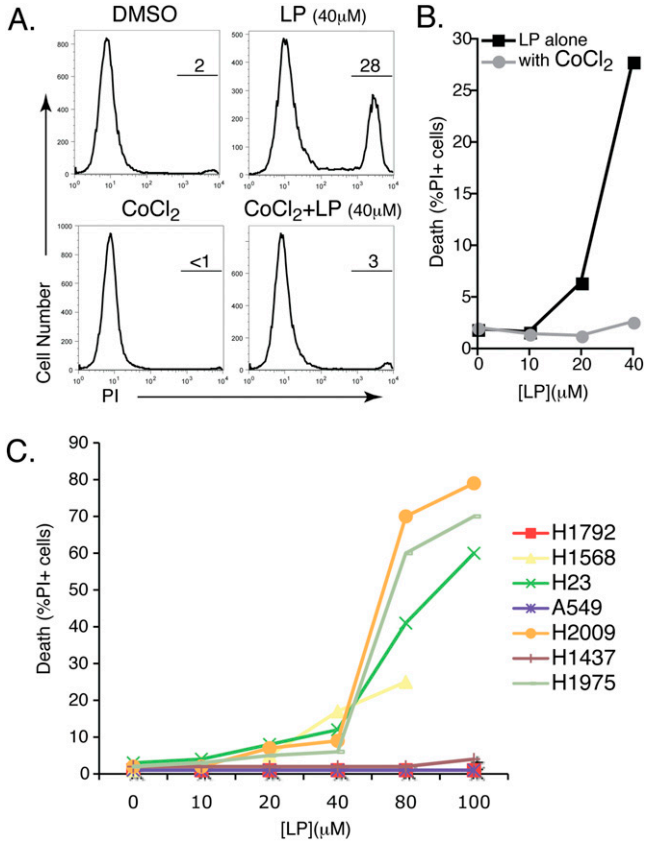

Fig. S10. LP kills *K-ras*^{G12D}-expressing sarcoma cells. (*A*) LP induced death of *K-ras*^{G12D}-expressing p53-deficient murine sarcoma cells is blocked by CoCl2. Data are representative of two independent experiments. (*B*) Inhibition of LP induced death of *K-ras*^{G12D}-expressing p53-deficient murine sarcoma cells by CoCl2 even at high doses of LP. (*C*) LP induces limited death of K-RAS mutant human lung cancer cell lines.

Table S1. GSEA of expression signatures of LP treatment in K-ras^{G12D} and wild-type MEFs

Lanperisone K-ras^{G12D} MEFs				Lanperisone wild-type MEFs			
Gene set	NES	*P*	FDR	Gene set	NES	*P*	FDR
Mense hypoxia up	3.28	<0.001	<0.001	Hypoxia reg up	2.68	<0.001	<0.001
Hypoxia review	2.89	<0.001	<0.001	Mense hypoxia up	2.56	<0.001	<0.001
Hypoxia reg up	2.82	<0.001	<0.001	Hypoxia review	2.45	<0.001	<0.001
Houstis ROS	2.66	<0.001	<0.001	Manalo hypoxia up	2.29	<0.001	<0.001
Schofield hypoxia	2.59	<0.001	<0.001	Hypoxia fibro up	2.19	<0.001	0.001
Manalo hypoxia up	2.57	<0.001	<0.001	HIF-1 targets	2.19	<0.001	0.001
HIF-1 targets	2.55	<0.001	<0.001	Glutathione met	2.04	<0.001	0.006
Oxstress breast CA	2.37	<0.001	<0.001	Oxstress breast CA	2.01	<0.001	0.010
Glutathione met	2.35	<0.001	<0.001	Hypoxia transporter	2.00	<0.001	0.010
Hypoxia fibro up	2.25	<0.001	<0.001	Houstis ROS	1.88	0.002	0.025

Gene sets shown demonstrated highly significant enrichment and are also annotated as being associated with either hypoxia or oxidative stress pathways (the latter highlighted in yellow). FDR, false discovery rate; NES, normalized enrichment score; *P*, permutation *P* value.